Synthesis of Ag-loaded tungsten oxide microspheres and their improved photocatalytic activity

Yu She[1], Yufu Zhu[1] ✉, Lei Zhou[2], Yuanmi Yuan[1], Jing Hao[1], Qingsong Jiang[3]

[1]*Faculty of Mechanical & Material Engineering, Huaiyin Institute of Technology, Huaian 223003, People's Republic of China*
[2]*Faculty of Mathematics and Physics, Huaiyin Institute of Technology, Huaian 223003, People's Republic of China*
[3]*Jiangsu Engineering Laboratory for Lake Environment Remote Sensing Technologies, Faculty of electronic information engineering, Huaiyin Institute of Technology, Huaian 223003, People's Republic of China*
✉ *E-mail: hyit2014@163.com*

Published in Micro & Nano Letters; Received on 11th July 2019; Revised on 19th September 2019; Accepted on 30th October 2019

In this study, tungsten oxide microstructures/nanostructures with different morphologies were prepared by the hydrothermal synthesis methods. The morphologies and structures of the obtained products were characterised by field-emission scanning electron microscopy and X-ray diffraction. The photocatalytic properties of tungsten oxide microstructures/nanostructures were characterised by the degradation of rhodamine B solution. The results indicate that tungsten oxide microspheres prepared by using tungstic acid and hydrogen peroxide solution as raw materials show the highest photocatalytic activity. By changing the concentration of tungstic acid used in the synthesis process, the morphologies of tungsten oxide microspheres can be controlled. The influences of the amount of chemical reagent addition on its morphology and catalytic properties were discussed. In order to further improve the photocatalytic activity of the samples, Ag nanoparticles were loaded on the obtained tungsten oxide microspheres. The photocatalytic experiment results indicate that the photocatalytic performance of tungsten oxide was improved by Ag loading. The results indicate that Ag-loaded tungsten oxide microspheres are favourable for their photocatalytic applications.

1. Introduction: Nowadays, environmental pollution has become an unavoidable problem in the development of human society. Semiconductor photocatalysis has the characteristics of high efficiency, low cost and no secondary pollution. It has become a research focus in the field of pollutant purification, renewable and sustainable materials [1]. The commonly used photocatalytic materials are mainly semiconductor oxides such as TiO_2 [2], WO_3 [3], ZnO [4] etc. Among them, TiO_2 and ZnO are the earliest and most studied, but they can only be excited under ultraviolet light, which limits their applications [5]. Therefore, visible light-activated catalysts have gradually become the focus of research in this field.

The current study found that the valence band edge potential of WO_3 is ~3.0 V_{NHE}, which provides sufficient driving energy for the hydroxyl radical reaction [6]. However, the conduction band edge potential (~0.4 V_{NHE}) of WO_3 is too high, which makes dissolved oxygen in the solution not be an effective electron acceptor, thus hindering the further reaction in the solution [7]. The oxygen molecules in the solution can hardly absorb the electrons generated by the photoexcitation of WO_3 effectively, which results in higher electron–hole recombination rate in the material, and will have some negative effects on the photocatalytic activity of the material [8].

In order to overcome these limitations, various techniques such as controlling material size [9], noble metal doping [10] and surface treatment were used to improve the catalytic activity [11]. A lot of researches have shown that noble metal doping can modify the bandgap energy of WO_3 and improve the electrical, optical and catalytic properties of materials [12]. When WO_3 is loaded with Au, Pt and Ag, the visible light absorption scope of WO_3 is broadened [13]. Among the various above-mentioned noble metal loaded on WO_3, silver nanoparticles (Ag NPs) have attracted wide attention because of their low price and good antibacterial properties. Although there have been reports on the modification of WO_3 with Ag NPs as catalysts, sensors, photoelectrochemical materials and photocatalysts, few reports have systematically studied the effect of morphology, structure and Ag doping on the photocatalytic properties of tungsten oxide [14]. In this paper, the synthesis of tungsten oxide microstructures/nanostructure with different morphologies and structures was realised. The photocatalytic properties of the obtained products were studied. The results show that the flower-like tungsten oxide microspheres exhibit excellent photocatalytic degradation activity. In order to further enhance the photocatalytic activity of tungsten oxide microspheres, Ag/WO_3 composites were prepared by photo-induced reduction method. The photocatalytic degradation experiment results show that the photocatalytic degradation activity of tungsten oxide microspheres was further improved by Ag loading.

2. Experimental section

2.1. Materials: Tungstic acid (H_2WO_4, 99%), citric acid ($C_6H_8O_7{\cdot}H_2O$, 99.995%), ammonium paratungstate ($(NH_4)_{10}[H_2W_{12}O_{42}]{\cdot}xH_2O$, 99%), sodium tungstate dihydrate ($Na_2WO_4{\cdot}2H_2O$, 99.5%), ammonium oxalate monohydrate ($(NH_4)_2C_2O_4{\cdot}H_2O$, 99.8%), silver nitrate ($AgNO_3$, 99.8%), rhodamine B (RhB) ($C_{28}H_{31}ClN_2O_3$) were purchased from Shanghai Aladdin Bio-Chem Technology Co., Ltd (China). Absolute ethanol (C_2H_6O, 99.5%), hydrochloric acid (HCl, 37%) and hydrogen peroxide aqueous solution (H_2O_2, 30%) were purchased from Sinopharm Chemical Reagent Co., Ltd (China). Cetyltri-methylammonium bromide (CTAB, 99%) was purchased from Nanjing Chemical Reagent Co., Ltd (China). All chemicals used in this study were of analytical grade and used without further purification.

2.2. Preparation of flower-like tungsten trioxide nanosheets: Flower-like tungsten trioxide nanosheets were prepared by a modified method given in [15]. First, 0.231 g sodium tungstate dihydrate ($Na_2WO_4{\cdot}2H_2O$) was dissolved in 30 mL deionised water. Under stirring conditions, 6 mL of 3M HCl solution was added drop by drop. The solution was stirred until there is no more white precipitation, and then 0.2 g ammonium oxalate monohydrate was added as the structure-directing agent. After stirring for a period of time till the solution became clear, the

doi: 10.1049/mnl.2019.0425

volume of the solution was adjusted to 70 mL by adding deionised water, and stirring for 30 min. The solution was transferred into two Teflon-lined stainless-steel autoclaves, sealed, placed in a constant temperature drying oven at 120°C for 12 h. After the reaction was finished, the obtained products were washed 3 to 4 times with deionised water and absolute ethanol. The products were dried at 60°C, and then calcined at 500°C for 1 h in air. The yielded products were denoted as Ns.

2.3. Preparation of bulk-like tungsten trioxide nanosheets: The bulk-like tungsten trioxide nanosheets were prepared by modifying a previously reported method given in [16]. First, 3 g of sodium tungstate dihydrate ($Na_2WO_4{\cdot}2H_2O$) and 0.005 g of CTAB were dissolved in 30 mL deionised water. Then 3 mL of the above solution was dripped into 5 mL of 3 M HCl and stirred for 30 min, the obtained yellow solution was transferred into Teflon-lined stainless-steel autoclaves and reacted at 100°C for 24 h. After cooling, the products were centrifuged and washed with distilled water and absolute ethanol for 3 to 4 times, respectively. The products were dried at 60°C and then placed in a muffle furnace at 500°C for 1 h to obtain yellow powder. The yielded products were denoted as Nb.

2.4. Preparation of spindle-like tungsten trioxide nanorods: First, 1.8 g of citric acid was dissolved in 140 mL of deionised water, and then 1 g of ammonium paratungstate was transferred into the above solution. After continuous stirring for 2 h, the solution became clear and transparent. Subsequently, the mixture was transferred into Teflon-lined stainless-steel autoclaves, then sealed and maintained at 160°C for 24 h. After the reaction, the products were centrifuged, washed with deionised water and absolute ethanol for several times, the products were dried at 60°C and calcined at 500°C for 1 h. The yielded products were denoted as Nr.

2.5. Preparation of flower-like tungsten oxide nanospheres: First, 1.125 g of tungstic acid powder was ultrasonically dispersed in a mixture of 90 mL of deionised water and 30 mL of hydrogen peroxide solution. The solution became clear after magnetic stirring at room temperature for 24 h. Then, the above solution was transferred into Teflon-lined stainless-steel autoclaves, sealed, and placed at 180°C for 2 h. The obtained products were washed several times with deionised water and absolute ethanol by centrifugal sedimentation, then dried at 60°C and calcined at 500°C for 1 h. The obtained samples were denoted as Nf. A series of tungsten oxide nanospheres were prepared by changing the amount of reagent added in the solution (0.214, 0.375, 0.563 and 2.550 g in 90 mL deionised water and 30 mL hydrogen peroxide mixed solution) and the obtained products were recorded as Nf-1, Nf-2, Nf-3 and Nf-4, respectively.

2.6. Preparation of silver/tungsten oxide composite nanospheres: First, 50 mg of the synthesised flower-like tungsten oxide nanospheres were dispersed in a mixture of 15 mL of absolute ethanol and 0.04 g of $AgNO_3$. After ultrasonic dispersion for 10 min, the mixture was irradiated by a 300 W xenon lamp for 1 h with continuous stirring. The mixture was collected by centrifugation, dried in a vacuum oven at 50°C, and then sintered at 500°C for 1 h. A series of silver/tungsten oxide composite nanospheres were prepared by changing the amount (0.04, 0.06 and 0.08 g) of reagent used during the synthesis process, and were recorded as Nf/Ag-1, Nf/Ag-2 and Nf/Ag-3, respectively.

2.7. Characterisation: A field-emission scanning electron microscope (FESEM; Quanta 250 FEG) was used to investigate the morphologies of the synthesised samples. The elemental compositions of the samples were performed on an energy dispersive spectrometer (EDS; INCAX-Max 20; Oxford) and X-ray diffraction (XRD) patterns were recorded on a Bruker AXS Advanced X-Ray diffractometer system (D8 Advance; $2\theta = 15°–80°$), respectively.

2.8. Photocatalysis measurements: The photocatalytic activities of the obtained samples were evaluated by the degradation of RhB in an aqueous solution under simulated solar irradiation. The light source was a 300 W Xenon lamp (PLS-SXE300C). All samples were annealed at 500°C for 1 h before the photocatalytic experiments. In a typical experimental process, 7.5 mg of the sintered samples were dispersed in a 25 mL of 10 mg L^{-1} RhB solution. The suspending liquid was magnetically stirred in dark for 1 h before illumination to reach the adsorption–desorption equilibrium of RhB. During the experiment process, the distance between the xenon lamp and the reactor was maintained constant, and all catalytic experiments were carried out under a fixed light intensity. After the suspension was irradiated under simulated solar light, a fixed number of millimetres of liquids were taken out at certain time intervals, and the catalysts were removed by centrifugation. Finally, the liquid was placed in a dedicated cuvette and the changes of absorbance at the wavelength range of 350–900 nm were measured by a UV–vis spectrophotometer (Shimadzu UV-3600). To enhance the photocatalytic efficiency, 0.02 mL of 30% of H_2O_2 solution was added to the solution during the catalytic experiments of the silver/tungsten oxide composite nanospheres.

3. Results and discussion

3.1 Characterisation of flower-like tungsten trioxide nanosheets: Figs. 1*a* and *b* show the SEM images of the flower-like tungsten trioxide nanosheets (Ns) in low magnification and high magnification. As shown in Fig. 1*a*, it can be seen that the as-prepared Ns products were flower-like with an average diameter of about 3.5 μm. Due to the influence of ammonium oxalate monohydrate, numerous tungsten trioxide nanosheets aggregate into flower-like particles. High-magnification SEM images shown in Fig. 1*b* clearly demonstrates that the Ns samples were formed by the aggregation of nanosheets with a cross-sectional length of about 480 nm.

The typical EDS spectrum in Fig. 1*c* shows that the samples were composed of O and W elements. The result of XRD characterisation shown in Fig. 1*d* indicates that the obtained Ns samples are composed of monoclinic WO_3 (JCPDS Card No. 83–0951) [17]. Furthermore, no impurities were detected, indicating that the purity of the Ns samples is high. The diffraction peaks are sharp and strong, indicating that the synthesised sample is a better crystalline material.

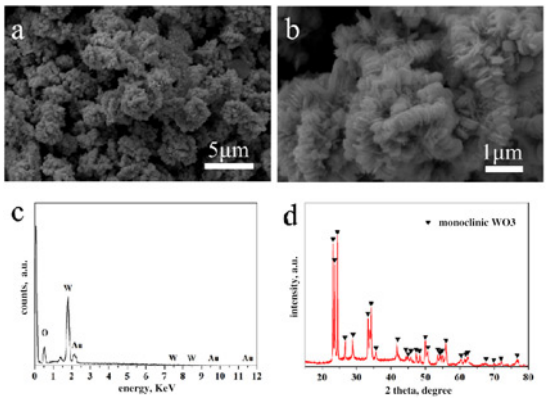

Fig. 1 *FESEM images and corresponding elemental analysis images of the Ns samples*
a Low magnification
b High magnification
c EDS spectrum
d XRD pattern

3.2. Characterisation of bulk-like tungsten trioxide nanosheets: The ammonium oxalate monohydrate was replaced by CTAB and the preparation process was modified to obtain the bulk-like tungsten trioxide nanosheets (Nb). The morphologies and sizes of the as-prepared Nb samples were evaluated by SEM. Figs. 2*a* and *b* show the SEM images of the Nb samples with different magnifications. The low magnification SEM image shows that a large quantity of bulk-like nanosheets was obtained. High-magnification SEM image presented in Fig. 2*b* indicates that the surface of the Nb samples is smooth with the average sizes of about 500–700 nm. The average thickness of the Nb samples is about 100 nm.

Fig. 2*c* demonstrates the EDS spectrum of the Nb samples, which indicates that the obtained bulk-like nanosheets mainly consist of O and W elements. The XRD pattern of Nb is shown in Fig. 2*d*. Based on the standard card of WO_3 crystal, all XRD diffraction peaks of Nb can be assigned to the monoclinic WO_3 (JCPDS Card No. 83–0951) [18]. No other impurity peaks appeared, indicating that the pure monoclinic WO_3 nanosheets can be synthesised by present method.

3.3. Characterisation of spindle-like tungsten trioxide nanorods: In order to systematically study the relationship between morphology and photocatalytic performance of tungsten oxide, different tungsten sources and methods were used to synthesise tungsten oxide with different morphologies. Figs. 3*a* and *b* show SEM images of spindle-like tungsten trioxide nanorods (Nr) with different magnifications. Fig. 3*a* indicates that the tungsten trioxide is mainly composed of short rod-like structures and its shape is similar to the spindles. High-magnification SEM image as presented in Fig. 3*b* clearly shows that the Nr samples have an average length of about 800 nm and a diameter of about 200 nm. Moreover, a large number of spindle-like structures with smaller sizes are distributed around them.

Fig. 3*c* indicates that the Nr samples contain two main elements of O and W. By analysing the XRD diffraction pattern shown in Fig. 3*d*, the diffraction peaks of Nr are consistent with the hexagonal WO_3 (JCPDS Card No. 33–1387) [19]. In the diffraction pattern of the sample, strong diffraction peaks appear at $2\theta = 22.72°$, 24.33°, 26.84°, 28.17°, 33.58°, 36.57°, 49.96° and 55.51°, which could be indexed to the (001), (110), (101), (200), (111), (201), (220) and (221) planes of the hexagonal WO_3, respectively. Therefore, the as-prepared Nr samples are composed of hexagonal tungsten trioxide.

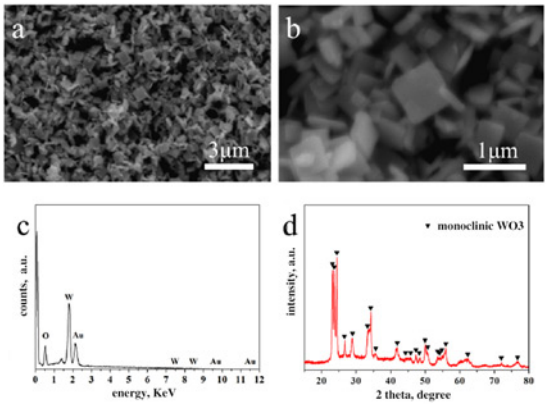

Fig. 2 *FESEM images and corresponding elemental analysis images of the Nb samples*
a Low magnification
b High magnification
c EDS spectrum
d XRD pattern

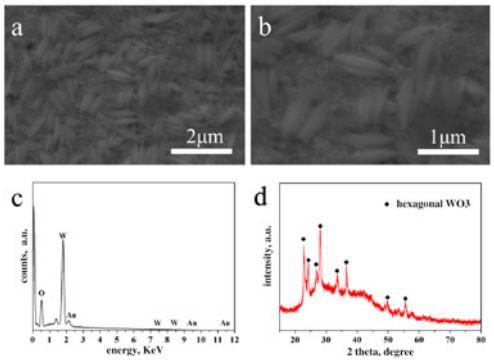

Fig. 3 *FESEM images and corresponding elemental analysis images of the Nr samples*
a Low magnification
b High magnification
c EDS spectrum
d XRD pattern

3.4. Characterisation of flower-like tungsten oxide microspheres: The flower-like tungsten oxide microspheres (Nf) were prepared by using tungstic acid as a tungsten source. Figs. 4*a* and *b* show SEM images of the obtained flower-like microspheres with different magnifications. The SEM image of the Nf samples shown in Fig. 4*a* indicates that the synthesised microspheres have a diameter of about 4 μm.

From the high magnification SEM image shown in Fig. 4*b*, one can find that the Nf samples are self-assembled by a large number of tungsten oxide short rods with rough surfaces. In addition, it also can be seen that there are numerous apertures between the nanorods. The EDS spectrum of Fig. 4*c* shows that the obtained samples mainly contain O and W elements. By analysing the XRD pattern (as shown in Fig. 4*d*), Nf is mainly composed of the orthogonal $WO_3{\cdot}0.33H_2O$ with strong diffraction peaks appear at $2\theta = 18.10°$, 23.07°, 24.17°, 28.11° and 36.67°. The diffraction peaks correspond to (111), (002), (200), (220), and (222) planes of the orthogonal $WO_3{\cdot}0.33H_2O$, respectively (JCPDS Card No. 72–0199) [20].

To investigate the photocatalytic activity of the as-obtained samples, photocatalytic degradation of RhB aqueous solution under simulated solar irradiation was carried out. Figs. 5*a–d* display the UV–vis absorption spectra of RhB solution degraded by tungsten oxide microstructures/nanostructures with different

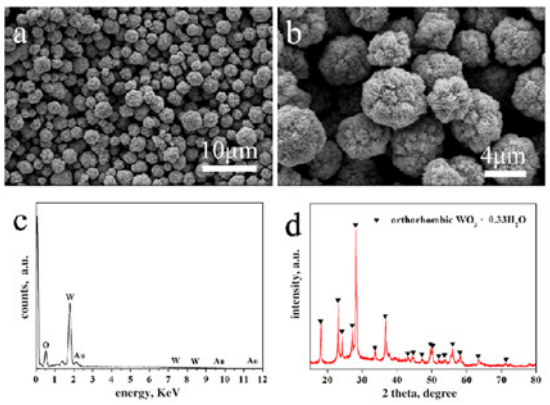

Fig. 4 *FESEM images and the corresponding elemental analysis images of the Nf samples*
a Low magnification
b High magnification
c EDS spectrum
d XRD pattern

doi: 10.1049/mnl.2019.0425

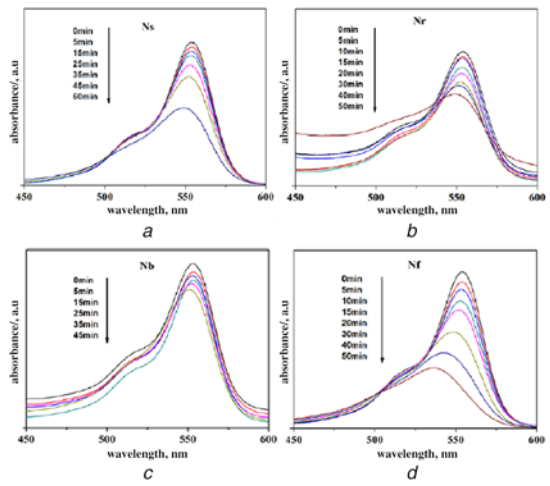

Fig. 5 *UV–vis absorption spectra changes of RhB solution photocatalysed by*
a Ns samples
b Nr samples
c Nb samples
d Nf samples

morphologies under simulated solar irradiation. From these figures, it is obvious that the absorbance of RhB decreases more rapidly under the degradation of the Nf samples compared with the other samples, which indicates that the Nf samples have a relatively rapid degradation rate.

To further investigate the photocatalytic activity of the flower-like tungsten oxide microspheres, a series of tungsten oxide microstructures/nanostructures with different morphologies were successfully synthesised by adjusting the amount of tungstic acid used during the synthesis process. The SEM images are shown in Figs. 6*a–d*. It can be seen from the figures that the addition amount of tungstic acid has a certain influence on the morphologies of the products. Fig. 6*a* shows that the Nf-1 samples are rugby-like structures with the length of about 2 μm and width of about 1.2 μm, and the surface consists of sheet-like structures. Fig. 6*b* shows that the morphologies of the Nf-2 samples, which are composed of star-shaped and spindle-shaped structures. The sizes of star-shaped structures are between 2.5 and 3 μm. The size of spindle-shaped structure is ~2.5 μm in length and 1.2 μm in width. Both of the structures are self-assembled by layers of smaller nanosheets. Fig. 6*c* shows the morphologies of the Nf-3 samples. It can be

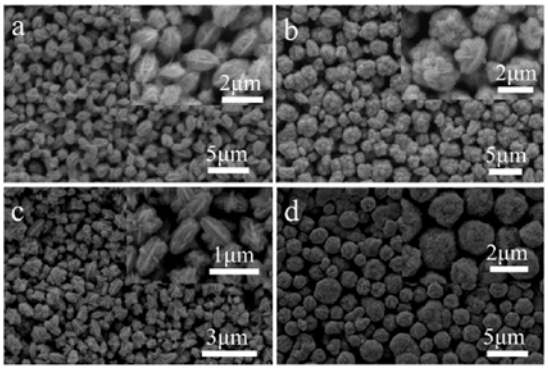

Fig. 6 *FESEM images of flower-like tungsten oxide microspheres with different amount of tungstic acid*
a 0.214 g
b 0.375 g
c 0.563 g
d 2.250 g

seen that the obtained samples are similar to balsam pear in shape, and the size is smaller than the Nf-2 samples. Its overall length is about 1 μm and the width is about 0.5 μm. The surface consists of tungsten oxide nanosheets with a thickness of about 100 nm. The morphology of the Nf-4 samples shown in Fig. 6*d* was similar to that of the Nf samples with a diameter of about 2 μm.

Figs. 7*a–d* display the UV–vis absorption spectra of RhB solution degraded by tungsten oxide microstructures/nanostructures with different morphologies under simulated solar irradiation. Fig. 8*a* shows the photocatalytic degradation efficiency of RhB in the presence of tungsten oxide microstructures/nanostructures with different morphologies and we found that the adsorption amount did not change much before illumination. The degradation kinetics of RhB aqueous solution according to UV–vis absorption spectra are displayed in Fig. 8*b*. The results were fitted using the formula $kt = \ln(C_0/C)$, where k, C_0 and C represent the slope of the line, the initial concentration and the concentration at different irradiation time of RhB solution, respectively [21]. The photocatalytic activity of the obtained samples can be analysed by

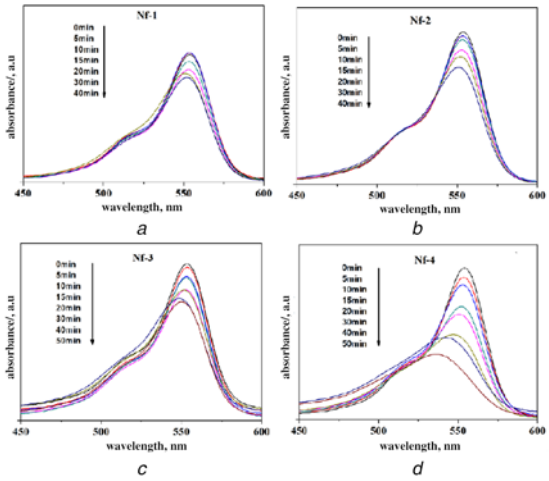

Fig. 7 *UV–vis absorption spectra changes of RhB solution photocatalysed by*
a Nf-1 samples
b Nf-2 samples
c Nf-3 samples
d Nf-4 samples

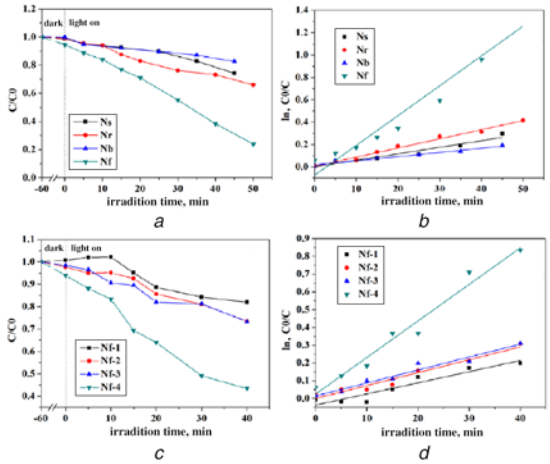

Fig. 8 *Related concentration changes and the corresponding degradation kinetic curves of RhB of*
a, b Ns, Nr, Nb and Nf samples
c, d Nf-1, Nf-2, Nf-3 and Nf-4 samples

comparing the slopes of the lines shown in Fig. 8*b*. The order of the degradation efficiencies of the obtained samples is as follows: Nf> Nr >Ns >Nb. Obviously, compared with the rod-like and flake-like tungsten oxide nanostructures, flower-like tungsten oxide microspheres exhibit higher photocatalytic performance. The reason can be attributed to the presence of nanopores and gaps on the surface of the Nf samples, and the unique morphology of the Nf samples may contribute to the improvement of the photocatalytic activity of tungsten oxide microspheres. Combined with the concentration changes and degradation kinetics curves shown in Figs. 8*c* and *d*, it can be concluded that the adsorption amount before illumination is still small and the Nf-4 samples exhibit the best photocatalytic degradation performance. By further comparing the degradation kinetic curves of the Nf-4 and Nf samples, the photocatalytic performance of the Nf samples is better than that of the Nf-4 sample.

3.5. Characterisation of silver/tungsten oxide composite microspheres: The obtained Nf samples were used to prepare the silver/tungsten oxide composite microspheres. From Fig. 9*a*, one can figure out that the diameter of tungsten oxide microspheres with Ag NPs prepared by photoinduced reduction method did not change too much compared with that of the Nf samples and it shows that the surfaces of the Nf/Ag-1 sample are covered with a layer of Ag NPs. With increasing the amount of $AgNO_3$ used during the synthesis process, one can find that the morphology of the samples did not change significantly, as shown in Figs. 9*b* and *c*.

To further elucidate the crystal structure of the composite microspheres, XRD results are shown in Fig. 9*d*. Further analysis revealed that the orthorhombic $WO_{1.09}$ (JCPDS Card No. 81–0558) diffraction peak appeared in the sample besides the peaks corresponding to $WO_3{\cdot}0.33H_2O$ (JCPDS Card No. 72–0199), which indicated that a small amount of incomplete tungsten oxide was produced during the sample preparation process, which was caused by the reduction of a small amount of tungsten trioxide to tungsten oxide in the heat treatment process [22]. At the same time, four extra diffraction peaks were observed at 38.2°, 44.4°, 64.6° and 77.6°. They can be indexed to (111), (200), (220) and (311) planes of Ag (JCPDS Card No. 87–0718) [23]. These results indicate that Ag NPs have been successfully deposited on the surface of the Nf samples. The element mappings of the Nf/Ag-1 composite microsphere as shown in Fig. 10 can also confirm the above result that the surfaces of the Nf/Ag-1 sample are covered with a layer of Ag NPs.

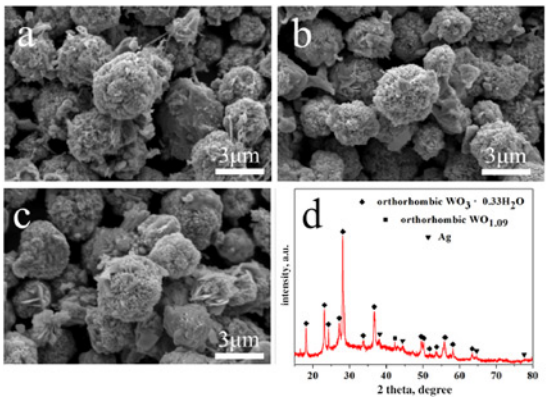

Fig. 9 *FESEM images of silver/tungsten oxide composite microspheres with different amount of silver nitrate*
a 0.04 g
b 0.06 g
c 0.08 g
d XRD pattern of the Nf/Ag-1 composite microspheres

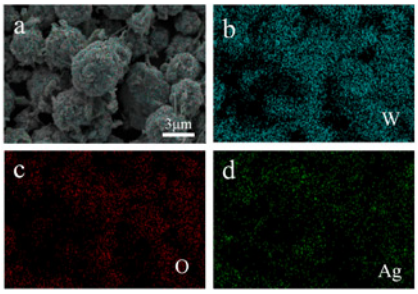

Fig. 10 *FESEM image with the element mappings of the Nf/Ag-1 composite microsphere and the corresponding elemental analysis images*
a SEM image with the element mappings
b–d the corresponding element mappings of W, O and Ag, respectively

3.6. Photocatalytic activity test: As the Nf samples have excellent photocatalytic properties, to further optimise the photocatalytic activity of the Nf samples, silver/tungsten oxide composite microspheres were successfully prepared. The UV–vis absorption spectra of silver/tungsten oxide composite microspheres with different amounts of $AgNO_3$ used during the synthesis process were displayed in Figs. 11*a–c*. During the photocatalytic activity test, a very small amount of H_2O_2 was also added in the solution to improve the degradation performance of the catalysts. The photocatalytic activity of unmodified tungsten oxide samples in the presence of H_2O_2 was added to show the role of silver (as shown in Fig. 11*d*). It was found that the Nf/Ag-1 sample had the best photocatalytic performance when the $AgNO_3$ addition amount was 0.04 g. The degradation time was shortened to less than one hour. It indicates that Ag loading improves the photocatalytic performance of the samples. This may be partially due to the surface plasmon resonance effect of Ag NPs [24]. In addition, incident photons are absorbed by WO_3 to generate electron–hole pairs. The photogenerated electrons will transfer to Ag NPs and lower the recombination rate of the electron–hole pairs [25]. The photogenerated electrons and holes can react with O_2 and H_2O adsorbed on the surface of the catalysts to form $\cdot O_2^-$ and ·OH radicals [6]. All the generated radical species can effectively decompose RhB dyes adsorbed on the surface of nanocomposite spheres [25]. However, compared with the indirect mechanism for dye

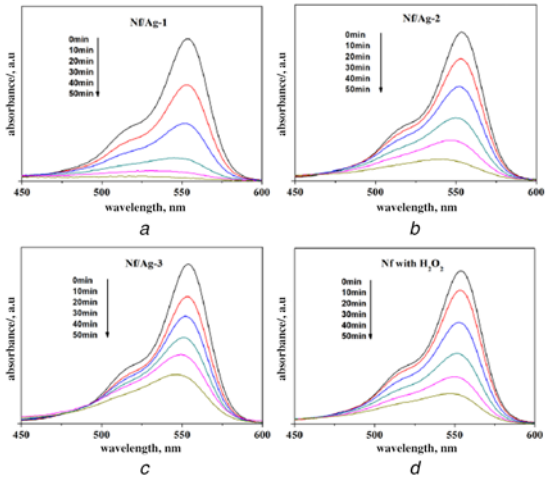

Fig. 11 *UV–vis absorption spectra changes of RhB solution photocatalysed by*
a Nf/Ag-1 samples
b Nf/Ag-2 samples
c Nf/Ag-3 samples
d Nf samples with H_2O_2

doi: 10.1049/mnl.2019.0425

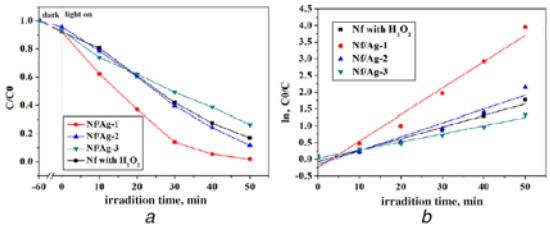

Fig. 12 *Related concentration changes and the corresponding degradation kinetic curves of RhB of*
a, b Nf with H_2O_2 sample and Nf/Ag-1, Nf/Ag-2, Nf/Ag-3 samples

degradation, the direct mechanism is considered to be a much slower reaction [26]. With the increase of silver nitrate used during the experimental process, the photocatalytic effect of the composite sample becomes worse, as displayed in Figs. 12*a* and *b*.

4. Conclusion: Tungsten oxide microstructures/nanostructures with different morphologies were successfully synthesised by the hydrothermal synthesis method. The photocatalytic properties of tungsten oxide microstructures/nanostructures with different morphologies were systematically investigated. Among the various tungsten oxide microstructures/nanostructures, the flower-like tungsten oxide microspheres exhibit a high photocatalytic degradation performance. The photocatalytic activity of the flower-like tungsten oxide microspheres was further improved by doping Ag NPs. Ag NPs on the tungsten oxide microsphere surfaces act as the electron trapping centres which could decrease the recombination rate of the electron–hole pairs and improve the photocatalytic performance of the tungsten oxide microspheres.

5. Acknowledgments: This work was supported by the Natural Science Foundation of Jiangsu Province (grant nos. BK20161300, BK20161303), the Six Talent Peaks Project in Jiangsu Province (grant nos. XNY-008, DZXX-011), the Qing Lan Project of Jiangsu Province, and also sponsored by the '333 Project' of Jiangsu Province.

6 References

[1] Crossland E.J.W., Noel N., Sivaram V., *ET AL.*: 'Mesoporous TiO_2 single crystals delivering enhanced mobility and optoelectronic device performance', *Nature*, 2013, **495**, (7440), pp. 215–219
[2] Zhao J., Zou X.X., Su J., *ET AL.*: 'Synthesis and photocatalytic activity of porous anatase TiO_2 microspheres composed of {010-faceted nanobelts', *Dalton Trans.*, 2013, **42**, (13), pp. 4365–4368
[3] Ke D., Liu H., Peng T., *ET AL.*: 'Preparation and photocatalytic activity of WO_3/TiO_2 nanocomposite particles', *Mater. Lett.*, 2008, **62**, (3), pp. 447–450
[4] Yu J., Yu X.: 'Hydrothermal synthesis and photocatalytic activity of zinc oxide hollow spheres', *Environ. Sci. Technol.*, 2008, **42**, (13), pp. 4902–4907
[5] Sakthivel S., Neppolian B., Shankar M.V., *ET AL.*: 'Solar photocatalytic degradation of azo dye: comparison of photocatalytic efficiency of ZnO and TiO_2', *Solar Energy Mater. Solar Cells*, 2003, **77**, (1), pp. 65–82
[6] Kim H., Kim H.N., Weon S., *ET AL.*: 'Robust Co-catalytic performance of nanodiamonds loaded on WO_3 for the decomposition of volatile organic compounds under visible light', *ACS Catal.*, 2016, **6**, (12), pp. 8350–8360
[7] Mcardle J.V., Hoffmann M.R.: 'Kinetics and mechanism of the oxidation of aquated sulfur dioxide by hydrogen peroxide at low pH', *J. Phys. Chem. B*, 1983, **87**, (26), pp. 5425–5429
[8] Miyauchi M.: 'Photocatalysis and photoinduced hydrophilicity of WO_3 thin films with underlying Pt nanoparticles', *Phys. Chem. Chem. Phys.*, 2008, **10**, (41), pp. 6258–6265
[9] Hidayat D., Purwanto A., Wang W.N., *ET AL.*: 'Preparation of size-controlled tungsten oxide nanoparticles and evaluation of their adsorption performance', *Mater. Res. Bull.*, 2010, **45**, (2), pp. 165–173
[10] Jansson I., Yoshiiri K., Hori H., *ET AL.*: 'Visible light responsive zeolite/WO_{3-Pt} hybrid photocatalysts for degradation of pollutants in air', *Appl. Catal. A Gen.*, 2016, **5**, (521), pp. 208–219
[11] Rahimnejad S., He J., Pan F., *ET AL.*: 'Enhancement of the photocatalytic efficiency of WO_3 nanoparticles via hydrogen plasma treatment', *Mater. Res. Express*, 2014, **1**, (4), p. 045044
[12] Zhang H., Huang C., Tao R., *ET AL.*: 'One-pot solvothermal method to synthesize platinum/$W_{18}O_{49}$ ultrafine nanowires and their catalytic performance', *J. Mater. Chem.*, 2012, **22**, (8), pp. 3354–3359
[13] Xu F., Yao Y., Bai D., *ET AL.*: 'Au nanoparticle decorated WO_3 photoelectrode for enhanced photoelectrochemical properties', *RSC Adv.*, 2015, **5**, (74), pp. 60339–60344
[14] Ghosh S., Acharyya S.S., Kumar M., *ET AL.*: 'One-pot preparation of nanocrystalline Ag–WO_3 catalyst for the selective oxidation of styrene', *RSC Adv.*, 2015, **5**, (47), pp. 37610–37616
[15] Qingyi Z., Li J., Bai J., *ET AL.*: 'Preparation of vertically aligned WO_3 nanoplate array films based on peroxotungstate reduction reaction and their excellent photoelectrocatalytic performance', *Appl. Catal. B Environ.*, 2017, **202**, pp. 388–396
[16] Meng D., Wang G., San X., *ET AL.*: 'CTAB-Assisted Hydrothermal synthesis of WO_3 hierarchical porous structures and investigation of their sensing properties', *Czechoslovak Math. J.*, 2015, **61**, (4), pp. 1077–1090
[17] Amano F., Li D., Ohtani B.: 'Fabrication and photoelectrochemical property of tungsten (VI) oxide films with a flake-wall structure', *Chem. Commun.*, 2010, **46**, (16), pp. 2769–2771
[18] Zhang J., Wang X.L., Xia X.H., *ET AL.*: 'Enhanced electrochromic performance of macroporous WO_3 films formed by anodic oxidation of DC-sputtered tungsten layers', *Electrochim. Acta*, 2010, **55**, (23), pp. 6953–6958
[19] Huirache-AcunA R., Paraguay-Delgado F., Albiter M.A., *ET AL.*: 'Synthesis and characterization of WO_3 nanostructures prepared by an aged-hydrothermal method', *Mater. Charact.*, 2009, **60**, (9), pp. 932–937
[20] Li L., Zhang D., Pu X., *ET AL.*: 'Hydrothermal synthesis and luminescent properties of $EuW_2O_6(OH)_3$ red micro-phosphors', *Adv. Powder Technol.*, 2011, **22**, (4), pp. 553–556
[21] Zhu Z., Yan Y., Li J.: 'One-step synthesis of flower-like WO_3/Bi_2WO_6 heterojunction with enhanced visible light photocatalytic activity', *J. Mater. Sci.*, 2016, **51**, (4), pp. 2112–2120
[22] Zaki M.I., Fouad N.E., Mansour S.A.A., *ET AL.*: 'Temperature-programmed and X-ray diffractometry studies of hydrogen-reduction course and products of WO_3 powder: influence of reduction parameters', *Thermochim. Acta*, 2011, **523**, (1–2), pp. 90–96
[23] Kim S.M., Jo Y.G., Lee S.Y.: 'The composition-controlled synthesis of Pt-Ag bimetallic nanochains for catalytic methanol oxidation', *Electrochim. Acta*, 2015, **174**, pp. 1244–1252
[24] Liu C., Yang D., Jiao Y., *ET AL.*: 'Biomimetic synthesis of TiO_2-SiO_2-Ag nanocomposites with enhanced visible-light photocatalytic activity', *ACS Appl. Mater. Interfaces*, 2013, **5**, (9), pp. 3824–3832
[25] Adhikari R., Gyawali G., Sekino T., *ET AL.*: 'Microwave assisted hydrothermal synthesis of Ag/AgCl/WO_3 photocatalyst and its photocatalytic activity under simulated solar light', *J. Solid State Chem.*, 2013, **197**, pp. 560–565
[26] Ajmal A., Majeed I., Malik R.N., *ET AL.*: 'Principles and mechanisms of photocatalytic dye degradation on TiO_2 based photocatalysts: a comparative overview', *RSC Adv.*, 2014, **4**, pp. 37003–37026.